



LAWRENCE
LIVERMORE
NATIONAL
LABORATORY

The energy coupling efficiency of multi-wavelength laser pulses to damage initiating defects in DKDP nonlinear crystals

P. DeMange, R A. Negres, A. M. Rubenchik, H. B. Radousky, M. D. Feit, S. G. Demos

September 25, 2007

Journal of Applied Physics

Disclaimer

This document was prepared as an account of work sponsored by an agency of the United States government. Neither the United States government nor Lawrence Livermore National Security, LLC, nor any of their employees makes any warranty, expressed or implied, or assumes any legal liability or responsibility for the accuracy, completeness, or usefulness of any information, apparatus, product, or process disclosed, or represents that its use would not infringe privately owned rights. Reference herein to any specific commercial product, process, or service by trade name, trademark, manufacturer, or otherwise does not necessarily constitute or imply its endorsement, recommendation, or favoring by the United States government or Lawrence Livermore National Security, LLC. The views and opinions of authors expressed herein do not necessarily state or reflect those of the United States government or Lawrence Livermore National Security, LLC, and shall not be used for advertising or product endorsement purposes.

**The energy coupling efficiency of multi-wavelength laser pulses to damage
initiating defects in DKDP nonlinear crystals**

P. DeMange, R. A. Negres, A. M. Rubenchik, H. B. Radousky, M. D. Feit, and S. G. Demos

Lawrence Livermore National Laboratory, 7000 East Ave., Livermore, CA 94550

(Received

ABSTRACT

The bulk damage performance of potassium dihydrogen phosphate crystals under simultaneous exposure to 1064-, 532-, and 355-nm nanosecond-laser pulses is investigated in order to probe the laser-induced defect reactions leading to damage initiation during frequency conversion. The results provide insight into the mechanisms governing the behavior of the damage initiating defects under exposure to high power laser light. In addition, it is suggested that the damage performance can be directly related to and predicted from the damage behavior of the crystal at each wavelength separately.

I. INTRODUCTION

With the development of evermore powerful lasers for scientific and technological applications, laser-induced damage in optical components within the laser system or the beam path is increasingly important. The understanding and control of damage initiation with ultrashort pulses has been achieved to a large extent,¹⁻³ primarily due to the fact that it is governed by intrinsic material properties. However, the nature of localized initiation of damage sites using nanosecond pulses still largely defies fundamental understanding despite more than four decades of research.^{4,5}

It is believed that the final stages leading to the formation of a damage site in optical materials for high power laser systems involve the formation of localized plasma and subsequent heating of the surrounding material.⁹ However, the origin of the localized absorption and mechanisms that govern the initiation of a damage event are unknown. The variation in the damage initiation threshold intensity observed with testing even between neighboring sites or using different beam sizes indicates the involvement of localized absorbing defect structures (referred to as damage precursors).

Potassium hydrogen phosphate (KH_2PO_4 or KDP) is one of the most studied materials due to its ease and quality of growth which has made it the prototype of choice for the investigation of hydrogen-bonded ferroelectrics as well as the model for crystal growth from a solution. Moreover, recent developments of growth methods that allow for the manufacturing of large size (~ 50 cm) KDP single crystals make this material and its deuterated analog, DKDP, the only nonlinear optical materials available for use in high-power, large-aperture laser systems (as Pockels cells, frequency converters and polarization control).^{6,7} Damage thresholds in these materials have increased over time, primarily due to purer raw materials and improvement in the

polishing and/or growth processes, though localized damage sites still arise from laser intensities far below that necessary to achieve dielectric breakdown.⁸ Many impurity and intrinsic stoichiometric defects have been identified in KDP/DKDP with chemical analysis and spectroscopic methods but efforts to correlate poor damage performance to their presence in increased relative concentrations have been inconclusive.^{8,10}

While previous work to evaluate the damage performance of materials for high-power lasers has focused exclusively on measuring their damage threshold,^{8,12} more recent work has employed damage testing approaches to investigate the entire population of the damage precursors. Within this new approach, the damage behavior is quantified in terms of the density of damage sites as a function of laser fluence and, thus, the damage threshold is only one point in this profile depicting the observed onset of damage arising from the precursors that initiate damage at the lowest fluence. However, laser-induced damage presents the most difficult issue to understand and predict during frequency conversion when multiple wavelengths are present at spatially and temporally changing relative fluencies. It is also during frequency conversion when higher-energy photons are generated which are known to represent a more significant threat.

In this work, we investigate the interaction leading to damage initiation of damage precursors with laser light under exposure to combinations of two wavelengths. This is achieved by measuring the density of damage sites created in the bulk of DKDP crystals under simultaneous exposure to the harmonics of a nanosecond-Nd:YAG laser at a matrix of fluence combinations and delay times. This is of practical interest because it approximates the conditions taking place during frequency conversion. The experimental results provide a) the means to predict performance under operationally relevant multi-wavelength irradiation conditions and b) insight

into the mechanisms governing damage initiation and the interaction of laser light with the absorbing defects responsible for damage.

II. EXPERIMENTAL PROCEDURE

The experiments were made possible using the new approach to evaluating the damage performance of a material in which the density of damage sites (pinpoint density or PPD) formed in the bulk following exposure to laser pulses is directly measured. Figure 1 shows an illustration of the experimental arrangement. The damage testing is performed using the fundamental (at 1064 nm), second, and third harmonics of a pulsed Nd:YAG laser having pulse durations (at FWHM of the temporal intensity profiles) of 5.8, 4.0, and 2.5 ns, respectively. High reflectivity mirrors selective to each wavelength are used to separate each harmonic of the output beam. The energy of each harmonic beam is controlled using a waveplate (WP) and polarizer (POL) combination. The three beams are then aligned to co-propagate and focused by cylindrical lenses ($f = 200$ mm) to the bulk of the material. Galilean telescopes (TS) are placed in each beam path to 1) decrease the diameter of each beam to ~ 2.5 mm and 2) correct for differences of the index of refraction of the cylindrical lens at each wavelength in order to focus each beam at the same location within the sample bulk. The spatial profiles of each beam are measured using a CCD-based beam profiling system with a spatial resolution of ~ 5 μm . All beams are focused to a $1/e^2$ height of 2.5 mm (± 0.15 mm) and widths of 50, 81, and 58 μm (± 2 μm) for 1064, 532, and 355 nm, respectively. The temporal overlap of the laser pulses at each harmonic was achieved by keeping the distances of the beam paths the same. Due to the significant difference in index of refraction at 1064 nm by the focusing cylindrical lens compared to the other two wavelengths (532 and 355 nm), the 1064-nm beam was focused by a separate cylindrical lens through the

back of the sample (as shown in Fig. 1). To obtain a temporal delay between laser pulses at different harmonics, a beam splitter is used to send half of the pulse along a delay path before recombining with the main path for delay times up to 20 ns.

The damage sites were illuminated with a counter-propagating 632.8-nm He-Ne laser beam focused by a cylindrical lens ($f = 250$ mm) through the back of the samples to overfill the tested volume. A CCD camera captured images of the scattered 632.8-nm laser light from the damage sites through the side of the sample, orthogonally to the laser beam path, using a microscope system equipped with a long-working-distance objective lens. The total number of damage sites is counted over the region of the volume exposed to peak laser fluence ($\pm 5\%$), a height of ~ 340 μm and length of 5.8 mm. The $1/e^2$ of the width of the pulsed beam was used as the depth in calculating the volume for determining the PPD in all experiments. This corresponded to a volume of ~ 0.15 mm^3 . More information on the entire range of capabilities of this experimental system can be found in Ref. 13.

The DKDP samples used in this work were $1 \times 5 \times 5$ cm^3 size plates polished on all sides. They were obtained from larger plates that were cut for third harmonic generation from conventionally grown crystals. The plane containing the crystal axis was situated horizontally for each sample while the polarization of each harmonic beam was rotated to vertical when necessary in order to be orthogonal to the crystal axis.³

Three sets of experiments were performed involving a) damage testing of bulk material to spatially and temporally overlapping pulses at 532 and 355 as well as b) 1064 and 355 nm in various fluence combinations and c) the 355-nm pulse delayed with respect to the 532-nm pulse between 0-10 ns. Experiments were performed using samples that were obtained from three crystal boules that exhibited different damage performance. The measured PPD following

exposure of DKDP samples from different boules at a particular fluence combination varied but the observed behaviors were the same. The results shown here are all obtained from samples taken from the same crystal boule.

III. EXPERIMENTAL RESULTS

The damage performance under simultaneous exposure to 532- and 355-nm pulses was quantified as the measured PPD using a matrix of fluences at each wavelength. This 3-dimensional data set is shown in Fig. 2 plotted as a function of the 532-nm fluence (Fig. 2a) and the 355-nm fluence (Fig. 2b). The data are displayed as PPD profiles at fluences of 0, 3, 5, 8, 10, 12, 15, and 20 J/cm² at 355 nm in Fig. 2(a) and PPD profiles at fluences of 0, 5, 8, 12, 16, 20, and 24 J/cm² in Fig. 2(b). The PPD versus fluence under exposure to each wavelength separately are also included for comparison and displayed as data at 0 J/cm² at the complementary wavelength.

Figure 3 shows the damage behavior under simultaneous exposure to a combination of fluences at 0, 6, 10, 14, 21.5, 26.5, 35, 45, and 50 J/cm² at 1064 nm and 4, 6, 8, 10, 12, and 14 J/cm² at 355 nm. The data are displayed as PPD profiles as a function of the 1064- (355-) nm fluence in Fig. 3(a) (Fig. 3(b)). The PPD versus fluence under exposure to 355 nm only is also shown for comparison and is displayed as a profile at a constant fluence of 0 J/cm² in Fig. 3(b). Exposure to pulses at 1064 nm only did not result in damage over the entire range of fluences used in the experiment. In all data shown in Figs. 2 and 3, individual data points represent the average PPD of four tested volume sites at that combination of fluences at both wavelengths.

The damage behavior when one of the two pulses is delayed with respect to the other (pump-probe) was also investigated in order to obtain information regarding the temporal evolution of the excitation process leading to damage initiation. These experiments were performed using the 532-nm pulse preceded by the 355-nm pulse. We used this sequence of pump and probe pulses in order to avoid “conditioning” of the damage precursors from the first pulse which would affect its interaction with the trailing pulse.¹⁴ Inter-pulse delay times of 0 up to 10 ns were used and the resulting PPD was measured for each delay and for several pulse fluence combinations at each wavelength. However, the fluences were chosen so that the PPD measured at 0 ns delay (simultaneous exposure) was high enough to differentiate it from the PPD resulting from individual pulse exposure.

Figure 4 shows the results for one combination of fluences of the pump and probe pulses. Specifically, the PPD resulting from 14 J/cm² at 532 nm followed by 7.5 J/cm² at 355 nm is plotted as a function of the delay time of the 355-nm (probe) pulse. At this combination of fluences, the PPD at 0 ns delay (simultaneous exposure) is ~ 900 pinpoints per mm³ (pp/mm³). The PPDs resulting from separate exposure at 14 J/cm² at 532 nm and 7.5 J/cm² at 355 nm were measured to be ~ 200 pp/mm³ and ~ 100 pp/mm³, respectively. Each data point is the average PPD of ten tested volumes and the error bars represent the standard deviation.

The results show that the PPD rapidly decreases from ~900 pp/mm³ as the inter-pulse delay is increased. For delay times of 5 ns and longer, the pulses were no longer overlapping and the PPD within these delay times was found to be ~ 200 pp/mm³. This is the same PPD as that measured from testing using only the 532-nm (pump) pulse as discussed above.

IV. ANALYSIS OF RESULTS

It is generally accepted that laser-induced damage in KDP/DKDP (and most other optical materials) is associated with the presence of an absorbing defect structure.⁸⁻²⁰ A yet unknown physical property of each precursor (such as size) determines the fluence at which each precursor will initiate damage. Independent of the absorption mechanism, it may be assumed that any given fluence at one wavelength may be related to an effective fluence at the other wavelength that provides equivalent absorption of energy by the precursors. This can be expressed as

$$E(\phi_{532}, \phi_{355}) = E(0, \phi_{355} + \phi_{355,eff}(\phi_{532}, \phi_{355})) \quad (1)$$

where $E(\phi_{532}, \phi_{355})$ is the absorbed energy by a precursor under simultaneous exposure to a fluence at 532 nm (ϕ_{532}) and fluence at 355-nm (ϕ_{355}), and $\phi_{355,eff}(\phi_{532}, \phi_{355})$ is the fluence at 355 that provides equivalent absorption corresponding to a given combination of fluences at both wavelengths. Equation (1) may be expanded by expressing the measured PPD (which quantifies the number of precursors that absorbed energy above a critical value) under simultaneous exposure to 532- and 355-nm as

$$\begin{aligned} PPD(\phi_{532}, \phi_{355}) &= PPD(0, \phi_{355} + \phi_{355,eff}(\phi_{532}, \phi_{355})) \\ &\approx PPD(0, \phi_{355} + \gamma_{355/532}(\phi_{532}, \phi_{355}) \cdot \phi_{532}) \end{aligned} \quad (2)$$

where $PPD(\phi_{532}, \phi_{355})$ is the measured PPD under simultaneous exposure, and $\phi_{355,eff}(\phi_{532}, \phi_{355})$ is the fluence at 355-nm that provides equivalent PPD corresponding to that provided at 532-nm.

The parameter $\gamma_{355/532}(\phi_{532}, \phi_{355})$ is defined as the ratio of the effective fluence at 355 nm over its corresponding fluence at 532 nm.

If $\gamma_{355/532}(\phi_{532}, \phi_{355})$, as expressed in Eq. (2), is independent of the fluence of the accompanying 355-nm pulse, applying Eq. (2) to our experimental results is equivalent to translating each PPD profile at constant 532-nm fluence by its $\phi_{355,eff}(\phi_{532})$ along the 355-nm fluence (horizontal) axis. To test this approach, we first measured the 355-nm only ($\phi_{532} = 0$) profile [as shown in Fig. 2(b)] over the full PPD range of the data and fit it to a power function. The best fit of all PPD profiles at constant 532-nm fluence [shown in Fig. 2(b)] were then fit to the 355-nm only PPD profile following translation of each profile along the 355-nm fluence axis. Figure 4 illustrates the fit of the data presented on a semi-log scale to better depict the damage behavior at both high and low PPD values. This figure demonstrates that each profile overlaps to a section of the 355-nm-only profile with a coefficient of determination (R^2) of 0.96 or greater along the fluence axis. The reasonable fit of each profile at constant 532-nm fluence to the 355-nm-only profile suggests that $\phi_{355,eff}(\phi_{532})$ (and thus $\gamma_{355/532}$), as measured and analyzed, is largely independent of the accompanying 355-nm fluence during simultaneous exposure.

Using the fitting procedure depicted in Fig. 5, the values of $\gamma_{355/532}$ for each profile at constant 532-nm fluence are extracted. These values of $\gamma_{355/532}$ as a function of the fluence at 532 nm are plotted in Fig. 6. The data shown as solid circles are deduced from the measurements presented in Fig. 2(b) while the data shown as open circles represent results from a second sample (from a different crystal boule) with a lower damage performance (higher PPD and lower damage threshold). Both sets of results illustrate identical behavior within experimental error. The error bars represent the extreme values of $\gamma_{355/532}$ obtained from fitting the edges of each

profile to the edge of 355-nm only profile (an R^2 along the fluence axis of better than 0.90 for each profile).

The same fitting procedure was tested for the experimental results shown in Fig. 3 for simultaneous damage testing with 1064- and 355-nm pulses with the PPD under simultaneous exposure expressed as

$$\begin{aligned} PPD(\phi_{355}, \phi_{1064}) &= PPD(0, \phi_{355} + \phi_{355,eff}(\phi_{1064})) \\ &\approx PPD(0, \phi_{355} + \gamma_{355/1064} \cdot \phi_{1064}) \end{aligned} \quad (3)$$

Figure 7 illustrates the best fit of each PPD profile at constant 1064-nm fluence to the profile from 355-nm only on a log-linear scale. Each profile overlaps to a section of the 355-nm-only profile with an R^2 of between 0.92 and 0.98. Similar to the previous case, the reasonable fit of the individual profiles to the 355-nm-only profile suggests that $\gamma_{355/1064}$, as analyzed, is independent of accompanying 355-nm fluence during simultaneous exposure. Figure 8 shows the fitting values of $\gamma_{355/1064}$ for each PPD profile at constant 1064-nm fluence plotted as a function of the fluence at 1064 nm. The error bars again represent fitting the edges of each profile to the edge of 355-nm only profile (an R^2 along the fluence axis of better than 0.90 for each profile).

V. DISCUSSION

The results of this work provide information that can be used to evaluate the performance of KDP/DKDP material for harmonic conversion in which multiple wavelengths are present. The PPD resulting from simultaneous dual-wavelength exposure in both experiments (532- and 355-nm, and 1064- and 355-nm) is greater than the sum of the individual wavelength exposures, for all fluence combinations. For most fluence combinations in both experiments, the PPD is greater than twice the sum of PPDs from the individual wavelength exposures.

A model involving linear absorption at embedded nanoparticles (damage precursors) has been applied for over a decade to describe damage initiation for pulses longer than about 50 ps.¹⁵⁻¹⁹ Damage is associated with a nanoparticle having reached a critical temperature which results in localized mechanical and/or optical modification of the material.¹⁹ According to this model and the Mie theory^{19,21} considerations taken into account, the total energy E absorbed by a nanoparticle from each laser harmonic can be written as:

$$E \propto \pi a^2 \cdot Q_{532} \cdot \phi_{532} + \pi a^2 \cdot Q_{355} \cdot \phi_{355} \quad (4)$$

where $\phi_{532,355}$ refers to fluences at 532- and 355-nm, the Q 's refer to the absorption efficiencies of each precursor and πa^2 is the cross-section area of the nanoparticle. From this expression, a given fluence at 532 nm can be related to the effective fluence at 355 nm that provides equivalent absorption of energy at the nanoparticle (as discussed above) that is determined by the ratio of the absorption efficiencies at each wavelength:

$$\phi_{355,eff} = \frac{Q_{532}}{Q_{355}} \cdot \phi_{532} \quad \text{or} \quad \gamma_{355/532} = \frac{Q_{532}}{Q_{355}}. \quad (5)$$

In order to analyze our experimental results, we need to first recognize that the measured values of $\gamma_{355/532}$ and $\gamma_{355/1064}$ reflect the behaviors of the damage precursors that are at the threshold of damage initiation for the given set of fluences. The other precursors have been exposed to energy in excess of their damage threshold so that their behavior cannot be included when using energy balance equations.

Mie theory predicts that the absorption efficiency of nanoparticles depends on their size and the wavelength of the absorbed light, with absorption being introduced through the imaginary part of the index of refraction ($n = n_0 - ik$). Assuming that the larger particles will initiate damage at a lower laser fluence (as predicted by the absorbing nanoparticle model), the experimentally

observed behavior of $\gamma_{355/532} = \frac{Q_{532}}{Q_{355}}$ as a function of the particle size (or equivalently as a function of laser fluence) can be considered. We found that for imaginary parts of the index of refraction greater than 1, the results reproduced the same qualitative increase of the ratio with increasing fluence to that of $\gamma_{355/532}$ observed in Fig. 6 within a range of nanoparticle sizes smaller than about 100 nm. However, in this range of nanoparticle sizes, $\frac{Q_{532}}{Q_{355}}$ was restricted to values greater than 1. This would then indicate that the absorption at 532 nm is higher than that at 355 nm and therefore, the damage threshold fluence at 532 nm is lower than at 355 nm. The latter conclusion is in contradiction with the experimentally observed damage behaviors at these wavelengths (the damage threshold at 355 nm is always lower than that at 532 nm). Variation of this approach using different values of the real and imaginary part of the index of refraction at each wavelength does not alter this general behavior. Thus, the qualitative behavior predicted by the Mie theory within the linear absorption model does not agree with the experimental results shown in Fig. 6.

Recent experimental work has indicated that the absorption mechanism for damage initiation in KDP with 3-ns pulses over a wavelength range of ~310-535 nm involves a multi-photon process assisted by the presence of defect states within the band-gap.¹¹ This may suggest a modification to the absorbing nanoparticle model to assume nonlinear absorption as the primary mechanism for energy deposition at the precursor. In this case, the size of the precursor will still govern its damage initiation fluence (through heat diffusion) but the excitation conditions (such as density of populated excited states) present when the damage initiation conditions are met will be different for each precursor. Consequently, smaller precursors that damage at higher fluences will attain higher excitation conditions while their effective absorptivities (which are probed with

this experiment) will be more influenced by their excited state absorption characteristics. Therefore, the change of $\gamma_{355/532}$ with fluence can be attributed to a relative increase of the ratio of the excited state absorption coefficients at 532-nm and 355-nm compared to that of the ground state.

An analysis of the change of $\gamma_{355/1064}$ as a function of laser fluence similar to that presented above for $\gamma_{355/532}$ is not possible for two reasons. First, the overall contribution to the final PPD of the 1064-nm fluences is very small compared to that of the accompanying 355-nm fluence leading to very narrow range of effective 355-nm fluences. Specifically, the effective 355-nm fluence range is $\sim 2.5 \text{ J/cm}^2$ for the $\gamma_{355/1064}$ values shown in Fig. 8 compared to $\sim 22 \text{ J/cm}^2$ for the $\gamma_{355/532}$ values shown in Fig. 6. Second, the error bars for the $\gamma_{355/1064}$ values in Fig. 8 are larger compared to the mean value. As a result, it is not possible to determine with reasonable accuracy a functional dependence of $\gamma_{355/1064}$ on laser fluence. However, this experiment demonstrates that the contribution of the 1064-nm fluences in the absorption mechanism leading to damage initiation is very small compared to that of the shorter wavelengths. This is best illustrated by the values of $\gamma_{355/532}$ and $\gamma_{355/1064}$ (in Figs. 6 and 8, respectively) which, for the same effective 355-nm fluences, differ by a factor of ~ 10 . Moreover, the effective 355-nm fluence is less than 10% of that of the corresponding 1064-nm fluence. Thus, there is a small contribution from the 1064-nm fluence to the overall PPD during frequency conversion. This is put into perspective when one considers that it is typical for ns-pulsed lasers to have spatial or pulse-to-pulse fluence variations larger than 10%.

The $\gamma_{355/532}$ and $\gamma_{355/1064}$ profiles shown in Figs. 6 and 8, respectively, can be used to estimate the PPD during harmonic conversion in which a combination of fluences at any two or all of the three wavelengths are present. For example, fluences at 532 and 1064 nm can be

correlated to effective fluences at 355 nm. The PPD resulting from simultaneous exposure to any combination of fluences at all three wavelengths is then predicted from the PPD profile at 355-nm only according to the following equation:

$$\begin{aligned} &PPD(\phi_{355}, \phi_{532}, \phi_{1064}) \\ &= PPD(\phi_{355} + \phi_{355,eff}(\phi_{532}) + \phi_{355,eff}(\phi_{1064}), 0, 0) \end{aligned} \quad (6)$$

This predictive method can be applied by measuring only the PPD profile at one wavelength without having to perform the extensive damage testing under simultaneous exposure. The profiles of $\gamma_{355/532}$ shown in Fig. 6 obtained from two DKDP samples (cut from different crystal boules that exhibit very different damage characteristics) are within experimental error identical. This suggests that this profile may be applied to all DKDP crystals.

The experimental results provide additional insight into the different types of damage precursors. In Fig. 4, the PPD measured for delays 5 ns and longer (where the 532- and 355-nm pulses are no longer overlapping) is the same within experimental error to the PPD measured from only the 532-nm pulse. This suggests that the precursors that would result in damage by the 355-nm pulse (≈ 100 at this test 355-nm fluence) had already formed damage sites by exposure to the 532-nm pump pulse. That is, there is a large overlap of the damage precursor population giving rise to damage at 355-nm with that responsible for damage at 532-nm. This result is consistent with recent work on the different precursor populations involved in laser induced damage presented elsewhere.²⁰ It was also discussed in this previous work that the precursors give rise to damage in the same sequence with increasing fluence independent of the exposure wavelength. This can explain the behavior observed in Fig. 5 where the accurate fit of each profile at constant 532-nm fluence to the fit of the profile at 355-nm-only fluence (R^2 of 0.96 or greater) demonstrates that the former represents part of a single profile. This profile can be

related to the distribution of the precursor population with respect to their individual damage threshold which is independent of the wavelength.

The work presented in Ref. 20 also indicates that there exists a large non-overlap of the damage precursors at 1064 nm with those at 532 and 355 nm. However, damage testing at 1064 nm in the samples used in this work did not result in observation of damage over the entire range of fluences used (0-50 J/cm²). Thus, the PPD initiated under simultaneous exposure to 1064 and 355 nm is assumed to have arisen from the precursor population responsible for damage initiation at 532 and 355 nm. In this case, the fit of each profile at constant 1064-nm fluence to the fit of the profile at 355-nm-only depicts the behavior of only the precursors initiating damage at 532- and 355-nm. The small values of $\gamma_{355/1064}$ suggest the very small contribution of the 1064-nm photons on the excitation process leading to damage initiation. This behavior may be related to the electronic structure of the defects within the precursor.

The results of the pump-probe experiment shown in Fig. 4 provide information on the time evolution of the damage initiation mechanism. In particular, enhanced PPD is only observed for temporal overlap of the two pulses. This demonstrates that, within the temporal resolution of our experiment, there is no measurable effect that can be attributed to the “excitation” of the precursors by the pump pulse. Consequently, the decay time of the damage initiation process is shorter than ~1 ns. Assuming the absorbing nanoparticle model, these results suggest that the decay of the temperature of the particle due to heat diffusion is shorter than 1 ns, setting an estimated upper limit on its size of ~100 nm. On the other hand, assuming nonlinear absorption mechanism, these results may indicate that the decay of the excited state population is faster than our temporal resolution (as expected for electron-phonon relaxation processes). To resolve the exact absorption mechanism, a pump-probe experiment using shorter pulses may provide a

higher temporal resolution. However, the type of defects responsible for damage as well as the damage initiation mechanisms may not be the same to that governing damage with nanosecond pulses.

VI. CONCLUSIONS

The results clearly demonstrate synergetic damage effects in the presence of multiple wavelengths. As such, the damage effects during frequency conversion process must be considered, especially with regard to the development and operation of large-aperture laser systems for inertial confinement fusion experiments in which KDP/DKDP optical components will be implemented. The relative absorptivities between the three wavelength harmonics (1064, 532, and 355 nm) that are calculated in this work suggest that the damage performance during frequency conversion can be predicted using only the damage performance measured at a single wavelength. Nonetheless, the contribution of 1064 nm is small compared to that of 532- and 355-nm, both of which are the main contributors to the energy deposition leading to damage initiation.

ACKNOWLEDGEMENTS

This work was performed under the auspices of the U.S. Department of Energy by the University of California, Lawrence Livermore National Laboratory under contract W7405-Eng.48.

REFERENCES

- ¹A. P. Joglekar, H. Liu, E. Meyhofer, G. Mourou, A. J. Hunt, Proc. Natl. Acad. Sci. USA **101**, 5856 (2004).
- ²C. B. Schaffer, A. Brodeur and E. Mazur, Measurement Science and Technology, **12**, 1784 (2001).
- ³B. C. Stuart, M. D. Feit, S. Herman, A. M. Rubenchik, B. W. Shore, and M. D. Perry, Phys. Rev. B **53**, 1749 (1996).
- ⁴R. M. Wood, Laser-Induced Damage of Optical materials, IOP Publishing LTD (2003).
- ⁵X. A. Shen, S. C. Jones, and P Braunlich, Phys. Rev. Lett. **62**, 2711 (1989).
- ⁶J. J. De Yoreo, A. K. Burnham, P. K. Whitman, Int. Mater. Rev. **47**, 113-152 (2002).
- ⁷N. P. Zaitseva, J. Atherton, R. Rozsa, L. Carman, I. Smolsky, M. Runkel, R. Ryon, and L. James, J. of Crystal Growth, **197**, 911 (1999).
- ⁸A. K. Burnham, M. Runkel, M. D. Feit, A. M. Rubenchik, R. L. Floyd, T. A. Land, W. J. Siekhaus, and R. A. Hawley-Fedder, Appl. Opt. **42**, 5483 (2003).
- ⁹C. W. Carr, H. B. Radousky, A.M. Rubenchik, M.D. Feit, and S. G. Demos, Phys. Rev. Lett. **92**, 087401 (2004).
- ¹⁰S. G. Demos, M. Staggs, M. Yan, H. B. Radousky, and J. J. De Yoreo, “Investigation of optically active defect cluster in KH_2PO_4 under laser photoexcitation,” J. Appl. Phys. **85**, 3988–3992 (1999).
- ¹¹C. W. Carr, H. B. Radousky, and S. G. Demos, Phys. Rev. Lett. **91**, 127402 (2003).
- ¹²H. Yoshida, T. Jitsuno, H. Fujita, M. Nakatsuka, M. Yoshimura, T. Sasaki, and K. Yoshida, Appl. Phys. B **70**, 195 (2000).

¹³P. DeMange, C. W. Carr, H. B. Radousky, and S. G. Demos, Rev. Sci. Instrum. **75**, 3298 (2004).

¹⁴Conditioning refers to the improvement of the damage performance following exposure to laser irradiation. See P. DeMange, C. W. Carr, R. A. Negres, H. B. Radousky, and S. G. Demos, Opt. Lett. **30**, 221 (2005).

¹⁵R. W. Hopper, D. Uhlmann. Appl. Phys. **41**, 4023 (1970).

¹⁶S. I. Anisimov, V. A. Khokhlov, Instabilities in Laser-matter interaction, CRC Press Boca Raton, (1999).

¹⁷S. Papernov and A. W. Schmid, J. of Appl. Phys. **97**, 114906 (2005).

¹⁸F. Bonneau, P. Combis, J. L. Rullier, M. Commandre, A. Duing, J. Y. Natoli, M. J. Pellin, M. R. Savina, E. Cottancin, and M. Pellarin, Appl. Phys. Lett. **83**, 3855 (2003).

¹⁹M. D. Feit and A. M. Rubenchik, Laser induced damage in optical materials: 2003, Boulder Damage Symposium, SPIE, **5273**, 74 (2004).

²⁰P. DeMange, R. A. Negres, H. B. Radousky, and S. G. Demos, "Differentiation of defect populations responsible for bulk laser-induced damage in potassium dihydrogen phosphate crystals," Opt. Eng. **12**, 104205 (2006).

²¹Mie, G. "Beitraege zur Optik Trueber Medien, Speziell-Kolloidaler Metalosungen," Ann. Physik, **25**, 377-445 (1908).

FIGURE CAPTIONS

FIG. 1. Experimental arrangement. More details can be found in the text.

FIG. 2. Plots of the PPD resulting from simultaneous 532- and 355-nm fluence combinations: a) PPD profiles at constant 355-nm fluences versus 532-nm fluence and b) PPD profiles at constant 532-nm fluences versus 355-nm fluence.

FIG. 3. Plots of the PPD resulting from simultaneous 1064- and 355-nm fluence combinations: a) PPD profiles at constant 355-nm fluences versus 1064-nm fluence and b) PPD profiles at constant 1064-nm fluences versus 355-nm fluence.

FIG. 4. The PPD resulting from exposure to a 4.0-ns, 532-nm pulse followed by a 2.5-ns, 355-nm pulse versus delay time. A line is drawn through the data as a guide to the eye.


FIG. 5. The PPD profiles at constant fluence at 532 nm (left) are translated along the horizontal axis by suitable 355-nm fluences to achieve best fit to the 355-nm only PPD profile (shown with )

FIG. 6. The parameter $\gamma_{355/532}$ relating fluences at each wavelength providing equivalent PPD as a function of 532-nm fluence, for two different samples (open and solid data points).

FIG. 7. Best fit of PPD profiles at constant fluence at 1064 nm to the 355-nm only PPD profile (shown with ●).

FIG. 8. The parameter $\gamma_{355/1064}$, relating fluences at each wavelength providing equivalent absorption as a function of 1064-nm fluence.

Figure 1, DeMange et al.

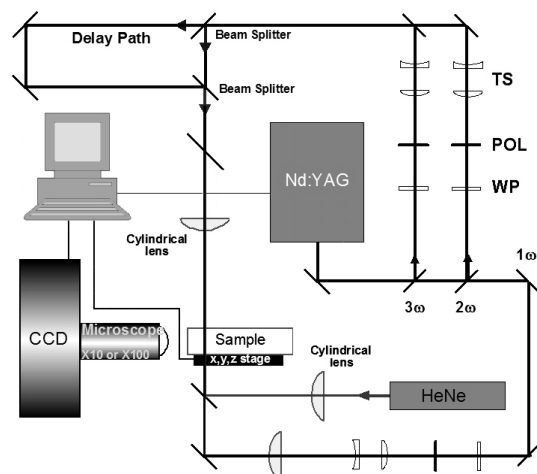


Figure 2, DeMange et al.

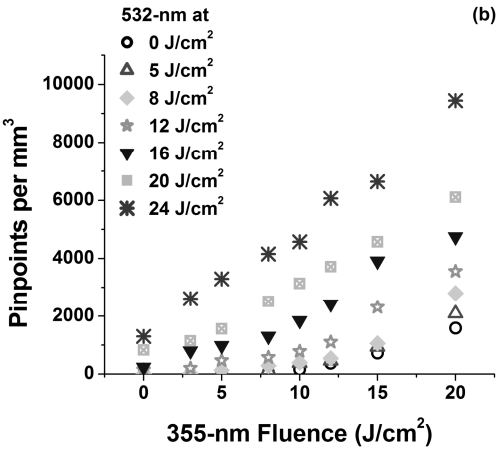
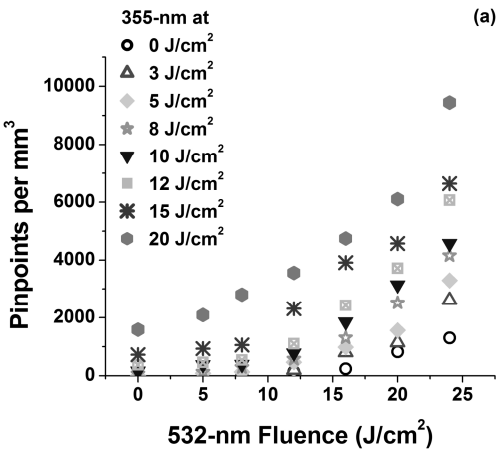


Figure 3, DeMange et al.

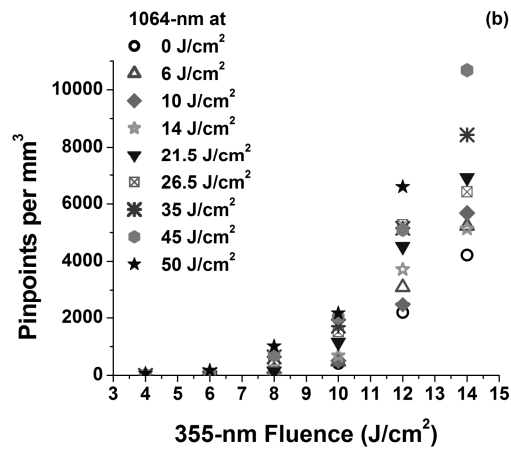
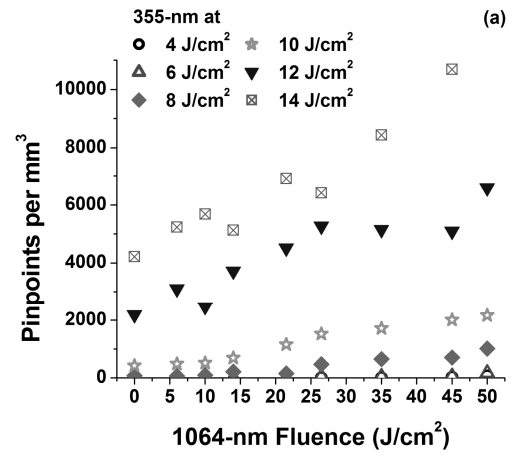


Figure 4, DeMange et al.

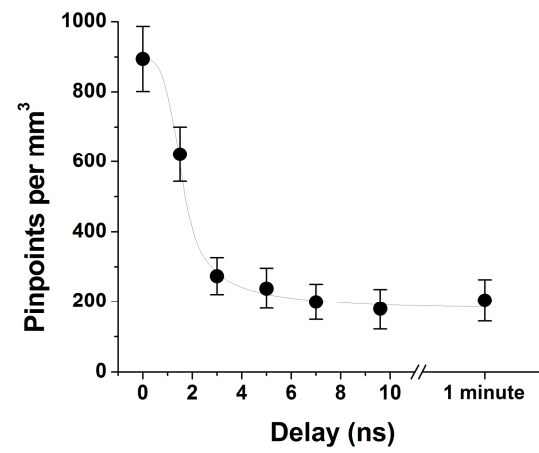


Figure 5, DeMange et al.

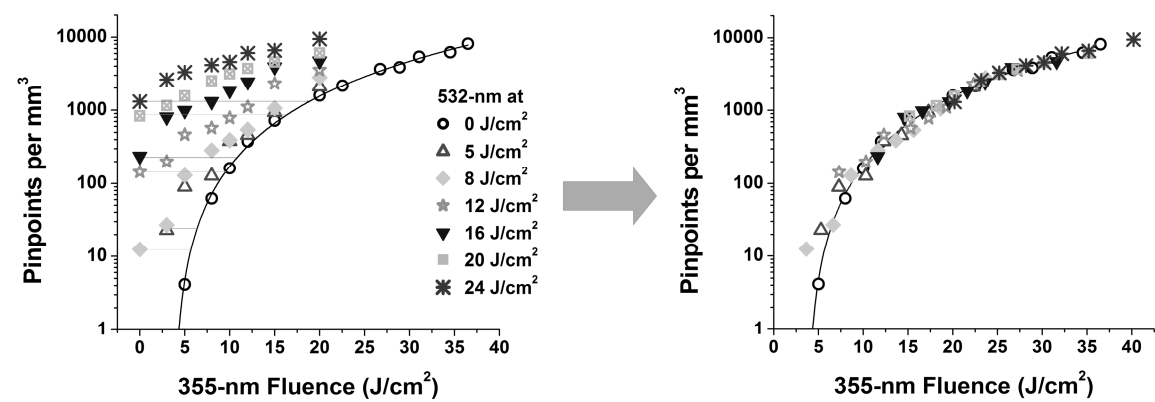


Figure 6, DeMange et al.

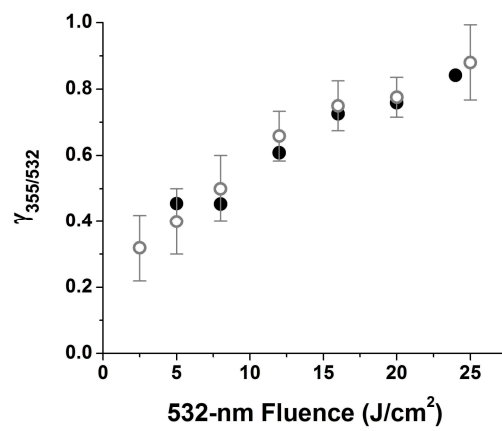


Figure 7, DeMange et al.

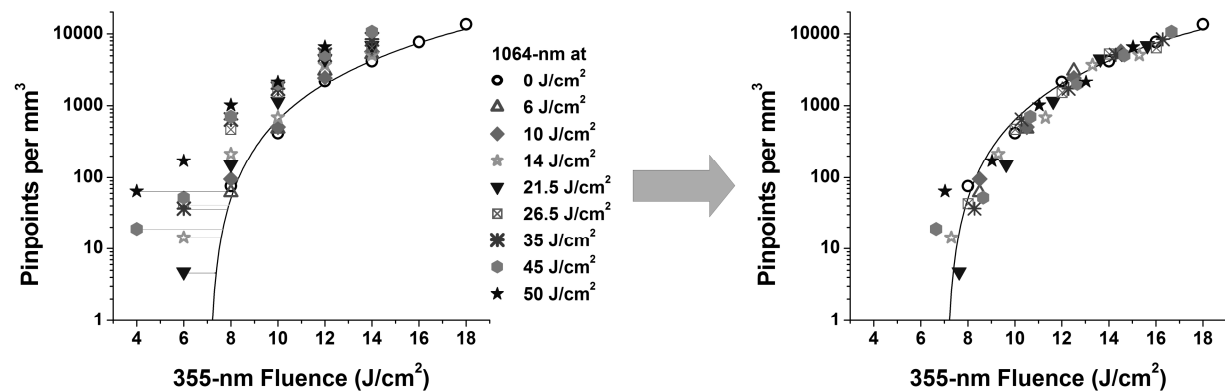


Figure 8, DeMange et al.

